Noname manuscript No.
(will be inserted by the editor)

Methane Activation by Heterogeneous Catalysis

Raimund Horn · Robert Schlögl

Received: date / Accepted: date

Abstract Methane activation by heterogeneous catalysis will play a key role to secure the supply of energy, chemicals and fuels in the future. Methane is the main constituent of natural gas and biogas and it is also found in crystalline hydrates at the continental slopes of many oceans and in permafrost areas. In view of this vast reserves and resources, the use of methane as chemical feedstock has to be intensified. The present review presents recent results and developments in heterogeneous catalytic methane conversion to synthesis gas, hydrogen cyanide, ethylene, methanol, formaldehyde, methyl chloride, methyl bromide and aromatics. After presenting recent estimates of methane reserves and resources the physico-chemical challenges of methane activation are discussed. Subsequent to this recent results in methane conversion to synthesis gas by steam reforming, dry reforming, autothermal reforming and catalytic partial oxidation are presented. The high temperature methane conversion to hydrogen cyanide via the BMA-process and the Andrussow-process is considered as well. The second part of this review focuses on one-step conversion of methane into chemicals. This includes the oxidative coupling of methane to ethylene mediated by oxygen and sulfur, the direct oxidation of methane to formaldehyde and methanol, the halogenation and oxy-halogenation of methane to methyl chloride and methyl bromide and finally the non-oxidative methane aromatization to benzene and related aromates. Opportunities and limits of the various activation strategies are discussed.

Keywords methane · heterogeneous catalysis · synthesis gas · steam reforming · dry reforming · autothermal reforming · partial oxidation · hydrogen cyanide · oxidative coupling · methanol · formaldehyde · halogenation · oxy-halogenation · aromatization

Prof. Dr. Raimund Horn
Institute of Chemical Reaction Engineering
Hamburg University of Technology
Eißendorfer Straße 38, 21073 Hamburg, Germany
Tel.: +49-(0)40-428-78-3242
Fax: +49-(0)40-428-78-2145
E-mail: horn@tuhh.de

Prof. Dr. Robert Schlögl
Department of Inorganic Chemistry
Fritz-Haber-Institute of the Max-Planck-Society
Faradayweg 4-6, 14195 Berlin
Tel.: +49-(0)30-8413-4400
Fax: +49-(0)30-8413-4685
E-mail: acsek@fhi-berlin.mpg.de

1 Introduction

Methane, CH_4, the most simple hydrocarbon, exists in enormous quantity on our planet. It occurs as the principal component of natural gas with a concentration between 70 % and 90 % by volume. According to the annually published BP Statistical Review of World Energy [1], proven world natural gas reserves were specified for the year 2013 to $187.3 \cdot 10^{12}$ m^3. Reserves denote only all that natural gas that can be recovered from known reservoirs under existing economic, technical and operating conditions. It does not include reservoirs yet to be discovered or natural gas which is currently too expensive for exploitation. In particular this number does not include natural gas found in crystalline hydrates at the continental slopes of many oceans and in permafrost areas. Estimates of the amount of methane stored in hydrates differ widely ranging from $2500 \cdot 10^{12}$ m^3 [2] to $15000 \cdot 10^{12}$ m^3 [3]. Methane chemistry experiences a boom not only because of its enormous reserves and resources but also because of improved production technology. Natural gas extraction

from shale rock in the United States by hydraulic fracturing triggered the so called 'shale gas revolution' [4]. Other countries in possession of huge shale gas resources, e.g. China, are currently following. Finally, methane is the main component of biogas formed by anaerobic digestion of energy crops, residues and wastes [5]. Depending on the raw material digested, methane concentration in biogas ranges from about 50 % to 70 % by volume. According to the 'EurObserv'er' barometer [6], biogas with a heating value of 10085.8 ktoe was produced in 2010 in the European Union corresponding to $1.1 \cdot 10^{10}$ m^3 natural gas. Today, biogas is almost exclusively used for energy production but bio methane could also become a chemical feedstock in the future.

Despite its vast availability, the use of methane as chemical raw material is still underrepresented. In particular, direct transformation routes of methane into chemicals and fuels, eliminating the expenses of intermediate synthesis gas generation, are missing. The majority amount of natural gas, more than 90 %, is burned to create energy for heating, cooking and transportation purposes or for electricity production. A declining but still significant amount of natural gas is flared in countries like Russia, Nigeria, Iran, Iraq and others. Estimates exist that about $100 \cdot 10^9$ m^3/year natural gas are flared world wide [7] which is about 3 % of the annual production of $3364 \cdot 10^9$ m^3/year [1]. If this number is compared to the percentage of natural gas used as chemical feedstock (less than 10 % of the world production), it can be seen that both numbers are of the same order.

The reason for this wasteful handling is of economic nature. The mass and energy density of natural gas ($\rho_{m,ng} \approx 0.7-0.9$ kg$\cdot$m^{-3}, $\rho_{e,ng} \approx 30-40$ MJ$\cdot$m^{-3}) is about three orders of magnitude lower than that of oil ($\rho_{m,oil} \approx 0.8-0.9$ kg$\cdot$dm^{-3}, $\rho_{e,oil} \approx 40$ MJ$\cdot$dm^{-3}) making handling and transportation in pipelines or LNG-tankers comparatively expensive. If economic conversion routes existed to convert natural gas/methane right at the wellhead into transportable liquids (methanol, gasoline...) less natural gas would be flared. Alternatively, more profitable conversion routes of natural gas into valuable chemicals at the consumer site would justify higher transportation costs as well. Unfortunately, apart from methane conversion to synthesis gas, hydrogen cyanide, acetylene and in minor amounts to chlorinated methane, industrial methane conversion pathways are not yet competitive to oil based production of chemicals and fuels. The purpose of this review is to provide a subjective account on today's methane chemistry with focus on heterogeneous catalysis.

2 Challenges in Methane Activation

Direct methane conversion into chemicals and fuels is often considered the 'holy grail' of chemistry and catalysis in the 21st century. Why is this so? Methane consists of a central carbon atom surrounded by four hydrogen atoms forming a regular tetrahedron (pointgroup T_d, C–H bond length 1.090 Å, bond angle $\angle 109.471°$). In the electronic ground state (X^1A_1), all electrons occupy binding molecular orbitals in a $(1a_1)^2(2a_1)^2(1t_2)^6$ electron configuration. The four C–H bonds are very stable ($\Delta_d H = 440$ kJ $\cdot$ mol^{-1}) and only weakly polarized. The carbon atom is slightly negatively charged ($\delta_C = -0.185$) and the hydrogen atoms are slightly positively charged ($\delta_H = +0.046$) (Hirshfeld method [8]). Due to symmetry, the dipole moment vanishes. Methane is resistant to nucleophilic attacks because electron donation into the high lying C–H σ^* orbital is energetically difficult and sterically hindered. Somewhat more facile but still challenging is the removal of electrons from the C–H σ bond by strong electrophiles. Methane has a very low proton affinity (544 kJ$\cdot$mol^{-1}) and is an extremely weak acid ($pK_a \approx 40$) rendering methane activation by acid/base catalysis difficult. The most facile way of methane activation is the homolytic C–H bond cleavage and hydrogen atom transfer to a radical as reaction partner. Schwarz et al. [9] reviewed thermal hydrogen atom transfer (HAT) from methane to oxygen centered gas-phase ion clusters and all gas-phase radical-ions possessing sufficient spin density at an oxygen atom were reactive in this transformation. Results of CH_4 oxidation to CH_3OH on Fe-ZSM-5 catalysts indicate that this mechanism could also be operational in heterogeneous catalysis[10].

Whatever way is chosen, drastic conditions such as high temperatures or aggressive reactants like superacids or radicals are almost inextricably linked to selectivity losses. If the inert CH_4 molecule can be activated, the more reactive target molecules will be even more readily activated.

The difficulties of methane activation discussed above are directly reflected in a small number of industrial conversion pathways. Direct methane conversion in industry is restricted to unselective radical chlorination to a mixture of CH_3Cl, CH_2Cl_2 and $CHCl_3$, methane partial combustion or electrothermal pyrolysis to acetylene and the reaction with ammonia to hydrogen cyanide. The latter can be carried out in presence of gas-phase oxygen (Andrussow-Process) or without oxygen (BMA-process). The most prominent use of methane in the chemical industry is for synthesis gas production by steam reforming, autothermal reforming or partial oxidation. The obtained CO/H_2 mixtures are used for

methanol or Fischer-Tropsch synthesis, hydroformulation reactions or the CO is removed to produce pure hydrogen for ammonia synthesis or hydrogenation reactions.

3 Progress in Heterogeneous Catalytic Syngas Production

Synthesis gas (short syngas), a mixture of H_2, CO and some CO_2, is a key intermediate in the chemical industry and is produced from methane catalytically by steam reforming, dry reforming, autothermal reforming or partial oxidation. The hydrogen used for ammonia production ($198 \cdot 10^6$ t NH_3 in 2012 [11]) and the syngas for methanol production ($65 \cdot 10^6$ t CH_3OH in 2013[12]) stems almost exclusively from natural gas, viz. methane. Increasing amounts of synthesis gas are needed for production of liquid fuels by Fischer-Tropsch synthesis ($40 \cdot 10^6$ t world GTL plant capacity 2011[13]).

Syngas production is a mature technology and has been discussed in detail in several excellent reviews [14–16] and books [17,18]. Only some recent developments, research results and challenges with focus on heterogeneous catalysis will be selected and discussed in the following.

3.1 Steam Reforming

In methane steam reforming, CH_4 reacts with H_2O to a mixture of CO, CO_2, H_2. The reaction is highly endothermic and limited by thermodynamic equilibrium. Two stoichiometrically independent reactions can describe the mole number changes of the five species involved, for example steam reforming (Eq. 1) and the watergas shift reaction (Eq. 2).

$$\mathrm{CH_4(g) + H_2O(g) \rightleftarrows CO(g) + 3H_2(g)} \quad (1)$$
$$\Delta H_r^\circ(298\ \mathrm{K}) = +206\ \mathrm{kJ \cdot mol^{-1}}$$
$$\mathrm{H_2O(g) + CO(g) \rightleftarrows CO_2(g) + H_2(g)} \quad (2)$$
$$\Delta H_r^\circ(298\ \mathrm{K}) = -41\ \mathrm{kJ \cdot mol^{-1}}$$

Steam reforming is catalyzed by group VIII transition metals. Both, experimental results and theroretical calculations show that Rh and Ru are the most active transition metals for steam reforming, Ni and Ir show intermediate activity and Pt and Pd are less active [19]. Co and Fe are also active but prone to oxidation under reaction conditions [14]. Ni based catalysts are used in industry due to the high price of Rh and Ru.

By combining DFT calculations, scaling relations and microkinetic modeling, Jones et al. [19] were able to calculate a 2D-volcano plot showing the turn over frequency as function of the O^* and C^* adsorption energies (Fig. 1). The calculated reactivity order was in line with experimental data presented in the same paper even though the TOF values were not quantitatively reproduced. TOF values increased linearly with dispersion indicating a structure sensitive reaction with stepped sites being more active than terrace sites. Jones et al. [19] also reported an elementary step mechanism for steam reforming on these metals and concluced that CO formation $C^* + O^* \rightleftarrows CO^* + *$ is the rate limiting step at the investigated temperature of 773 K but that dissociative CH_4 adsorption $CH_4 + 2* \rightleftarrows CH_3^* + H^*$ becomes rate limiting at higher temperatures in line with the experimental results obtained by Wei and Iglesia at $823 - 1023$ K [20].

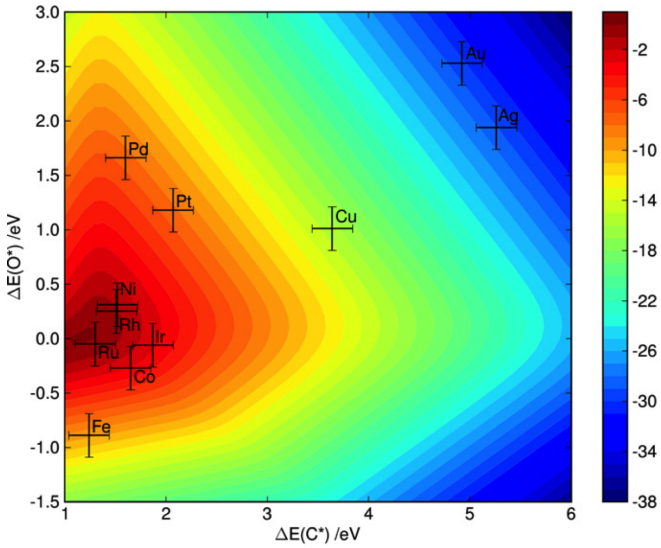

Fig. 1 Two-dimensional volcano-plot of the turn over frequency ($\log 10$) as a function of O and C adsorption energy. $T = 773$ K, $p = 1$ bar; 10 % conversion. The error bars include an estimated 0.2 eV uncertainties in the adsorption energies. Figure reproduced from Jones et al. [19]

The major challenge in steam reforming remains catalyst deactivation by i) sintering, ii) carbon blockage and iii) poisoning by S, As, Pb, P, SiO_2 and alkali metals. Much insight has been gained on Ni-deactivation from in situ TEM and DFT studies [14,21]. For example, Sehested [21] showed that Ni-deactivation occurs both by particle migration and coalescence but also by atom migration from small particles to larger particles (Ostwald ripening). DFT calculations gave evidence that Ni–OH is most likely the carrier for Ni-atom migration and a mathematical model for Ni-particle growth could be formulated [22]. Bengaard et al. [23] showed that graphene layer growth on Ni(111) originates from Ni(211) steps as nucleation sites. The same authors studied adsorption of K, S and Au on Ni-particles and there is theoretical evidence that these additives

bind to step sites as well. Hence it was concluded that minute amounts of these promotors could make steam reforming catalysts resistant to coking.

The examples listed above show how novel experimental and theoretical methods provide new insight into atomistic details of catalytic reactions and pave the way for improvements even to such established technologies like methane steam reforming.

3.2 Dry Reforming

In recent years, increasing environmental awareness, in particular with view on global warming, has rekindled interest in methane dry reforming (Eq. 3).

$$\mathrm{CH_4(g) + CO_2(g) \rightleftarrows 2CO(g) + 2H_2(g)} \qquad (3)$$
$$\Delta H_r^\circ(298\ \mathrm{K}) = +247\ \mathrm{kJ \cdot mol^{-1}}$$

In this highly endothermic reaction, two strong greenhouse gases, CO_2 and CH_4 are converted to syngas which can be used for methanol production or Fischer-Tropsch synthesis. In order to achieve a net CO_2 conversion, the heat of reaction must not be created by burning fossil fuels. Instead solar-thermal reactors are an interesting development [24] and could be used in the future. Aside from environmental aspects, methane dry reforming is of general interest to the chemical industry because it delivers a lower H_2/CO ratio than steam reforming which is desirable, e.g. if long chain hydrocarbons are to be produced by Fischer-Tropsch synthesis.

CH_4 activation, CO_2 activation and the reaction of both molecules on transition metal surfaces has been studied in great detail. Methane activation on transition metal surfaces is characterized by a high activation barrier, a low sticking coefficient and a high hydrogen kinetic isotope effect [25]. These features are attributed to a precursor mediated dissociation (PMD) mechanism of the rate limiting step in which $CH_4(ads) \rightarrow CH_3(ads) + H(ads)$ occurs by tunneling of an H atom through an energy barrier [25]. As shown in Figure 2, the rate constant for PMD follows a Brønsted-Evans-Polanyi relation with the total adsorption energy of a CH_3 fragment and an H atom as catalyst descriptors. At high kinetic energies (high temperatures) the precursor mediated dissociation shifts gradually to a direct dissociation (DD) mechanism as indicated by molecular beam and thermal bulb experiments of Seets et al. [26, 27]. Strong evidence exists that the reaction is structure sensitive[28].

CO_2 activation on transition metal surfaces is also a structure sensitive reaction. Broad agreement exists in

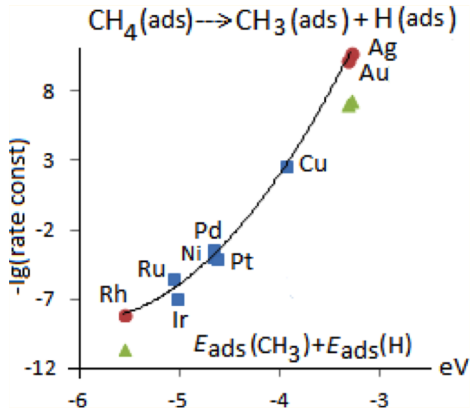

Fig. 2 BEP relationships between the rate constant (in s^{-1}) at $T = 500$ K and the sum of the H and CH_3 adsorption energies (in eV). Adopted from [25]

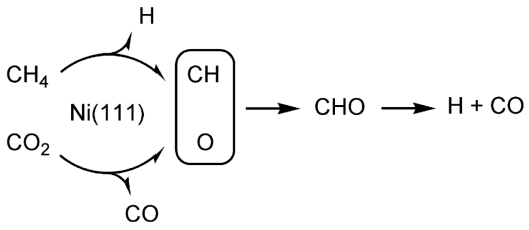

Fig. 3 Simplified Mechanism of CO_2 Reforming on Ni(111). Adopted from [30]

literature that CO_2 activation proceeds through electron donation from the transition metal to the CO_2 molecule forming a $CO_2^{\delta-}$ anion. Because a low work function enhances charge transfer, surface defects such as steps are more reactive than closed packed transition metal surfaces [29]. The $CO_2^{\delta-}$ precursor anion can only be observed far below room temperature. At reaction temperature of dry reforming CO_2 dissociates at the surface to CO and O. By means of DFT, Wang et al. [30] computed the entire reaction pathway and energetics for CO_2 reforming on Ni(111). According to their calculations, CO_2 dissociates at the surface to CO and O while CH_4 dissociates sequentially to CH + 3H. CH + O form CHO which splits off the remaining H atom. Figure 3 summarizes this simplified mechanism.

The biggest challenge for catalysis research in dry reforming is catalyst deactivation by carbon blockage. Both methane pyrolysis (Eq. 4) and the Boudouard equlibrium (Eq. 5) are potential sources of carbon formation [28]. Temperatures above 1000 K and excess CO_2 are required to reduce carbon formation [31].

$$\mathrm{CH_4(g) \rightleftarrows C(s) + 2H_2(g)} \qquad (4)$$
$$\Delta H_r^\circ(298\ \mathrm{K}) = +75\ \mathrm{kJ \cdot mol^{-1}}$$
$$\mathrm{2CO(g) \rightleftarrows C(s) + CO_2(g)} \qquad (5)$$
$$\Delta H_r^\circ(298\ \mathrm{K}) = -171\ \mathrm{kJ \cdot mol^{-1}}$$

While the closed packed and defect free Ni(111) surface is rather resistant with respect to carbon formation [30], steps, e.g. at Ni(211), are nucleation sites for carbon growth causing catalyst deactivation [32]. The calculations of Wang et al. [30] show that surface O and H atoms remove carbon deposits efficiently.

One currently followed approach to synthesize coking resistant dry reforming catalysts builds on the idea that very small metal nano-particles are less prone to coking than larger particles [33]. Perovskite based precursors such $La_{1-x}Sr_xNiO_3$, $La_{2-2x}Sr_{2x}NiO_{4-\delta}$, $LaNi_{1-x}Co_xO_3$ and $La_{1-x}Sr_xNi_{1-y}Co_yO_3$ release nanoparticles of the corresponding transition metals under CO_2 reforming conditions and show stable reforming activity and syngas selectivity at high CO_2 conversion [34].

3.3 Autothermal Reforming (ATR)

Low temperature FT-synthesis of wax and diesel on shift-inactive Co-catalysts requires syngas with a H_2/CO ratio close to 2.0 [35]. Oxygen-blown auto thermal reforming of natural gas (methane) is the syngas production method of choice for large-scale FT-plants. An ATR-reactor consists of a specially designed burner in which a sub-stoichiometric feed of natural gas, steam and oxygen ($H_2O/C = 0.5 - 3.5$, $O_2/C = 0.4 - 0.6$) is burned at temperatures of 2500 °C or more, a combustion chamber in which slower homogeneous gas-phase reactions like CO oxidation, steam reforming, watergas shift and pyrolysis occur and a heterogeneous catalytic zone in which methane and higher hydrocarbons are removed by steam reforming. The syngas leaving the ATR-reactor has a temperature between $850 - 1100$ °C, is in thermodynamic equilibrium and basically free of higher hydrocarbons and soot-precursors[14].

The catalyst used in ATR-reactors is in most cases Ni supported on magnesium alumina spinel ($MgAl_2O_4$). Due to the high operation temperature, ATR-catalysts are less prone to poisoning and deactivation than the Ni-catalyst in a primary steam reformer. Research challenges in ATR lie mainly in the field of reactor engineering and burner design. Challenges in catalyst design lie more on the side of minimizing pressure drop and finding the optimum pellet shape for minimizing intraparticle transport than on new catalyst formulations.

3.4 Catalytic Partial Oxidation

Catalytic **P**artial **O**xidation (**CPO**) of methane is a promising but not yet industrially applied method for converting methane to synthesis gas. In CPO, methane and oxygen (or air) are premixed and converted in a catalytic fixed bed reactor to a mixture of H_2 and CO in a ratio of nearly 2 : 1, favorable for downstream methanol oder FT-synthesis. H_2O and CO_2 are side products. Catalysts for CPO are group VIII noble metals such as Rh, Pt, Pd, Ir, Ru and non-noble metals like Ni and Co. Enger et. al. [36] listed reactions that are thought to play a role in methane CPO.

$$CH_4(g) + 2O_2(g) \rightarrow CO_2(g) + 2H_2O(g) \quad (6)$$
$$\Delta H_r^\circ(298\ \mathrm{K}) = -803\ \mathrm{kJ \cdot mol^{-1}}$$
$$CH_4(g) + 1/2O_2(g) \rightarrow CO(g) + 2H_2(g) \quad (7)$$
$$\Delta H_r^\circ(298\ \mathrm{K}) = -36\ \mathrm{kJ \cdot mol^{-1}}$$
$$CH_4(g) + O_2(g) \rightarrow CO_2(g) + 2H_2(g) \quad (8)$$
$$\Delta H_r^\circ(298\ \mathrm{K}) = -319\ \mathrm{kJ \cdot mol^{-1}}$$
$$CO(g) + H_2O(g) \rightleftarrows CO_2(g) + H_2(g) \quad (9)$$
$$\Delta H_r^\circ(298\ \mathrm{K}) = -41\ \mathrm{kJ \cdot mol^{-1}}$$
$$CH_4(g) + H_2O(g) \rightleftarrows CO(g) + 3H_2(g) \quad (10)$$
$$\Delta H_r^\circ(298\ \mathrm{K}) = +206\ \mathrm{kJ \cdot mol^{-1}}$$
$$CH_4(g) + CO_2(g) \rightleftarrows 2CO(g) + 2H_2(g) \quad (11)$$
$$\Delta H_r^\circ(298\ \mathrm{K}) = +247\ \mathrm{kJ \cdot mol^{-1}}$$
$$CO(g) + H_2(g) \rightleftarrows C(s) + H_2O(g) \quad (12)$$
$$\Delta H_r^\circ(298\ \mathrm{K}) = -131\ \mathrm{kJ \cdot mol^{-1}}$$
$$CH_4(g) \rightleftarrows C(s) + 2H_2(g) \quad (13)$$
$$\Delta H_r^\circ(298\ \mathrm{K}) = +75\ \mathrm{kJ \cdot mol^{-1}}$$
$$2CO(g) \rightleftarrows CO_2(g) + C \quad (14)$$
$$\Delta H_r^\circ(298\ K) = -172\ \mathrm{kJ \cdot mol^{-1}}$$
$$CO(g) + 0.5O_2(g) \rightarrow CO_2(g) \quad (15)$$
$$\Delta H_r^\circ(298\ \mathrm{K}) = -283\ \mathrm{kJ \cdot mol^{-1}}$$
$$H_2(g) + 0.5O_2(g) \rightarrow H_2O(g) \quad (16)$$
$$\Delta H_r^\circ(298\ \mathrm{K}) = -242\ \mathrm{kJ \cdot mol^{-1}}$$

In literature, syngas formation by methane CPO ist often discussed in terms of a direct partial oxidation route (Eq. 7) vs. a combustion-reforming route (combination of Eq. 6, Eq. 10 and Eq. 11). From reactor exit data, which are often close to thermodynamic equilibrium, the syngas formation pathway cannot be judged. Spatial profile measurements through adiabatically operated Rh and Pt coated $\alpha - Al_2O_3$ foam catalysts show that H_2 and CO are formed in a short oxidation zone at the entrance of the foam and upon complete O_2 consumption by steam reforming [37]. CO_2 reforming (Eq. 11) was not observed. The formation of H_2 in presence of gas-phase O_2 is due to a strong film transport limitation leading to a vanishing O_2 concentration at the catalyst surface [38]. Spatially resolved XAS-measurements show the Rh oxidation state as function

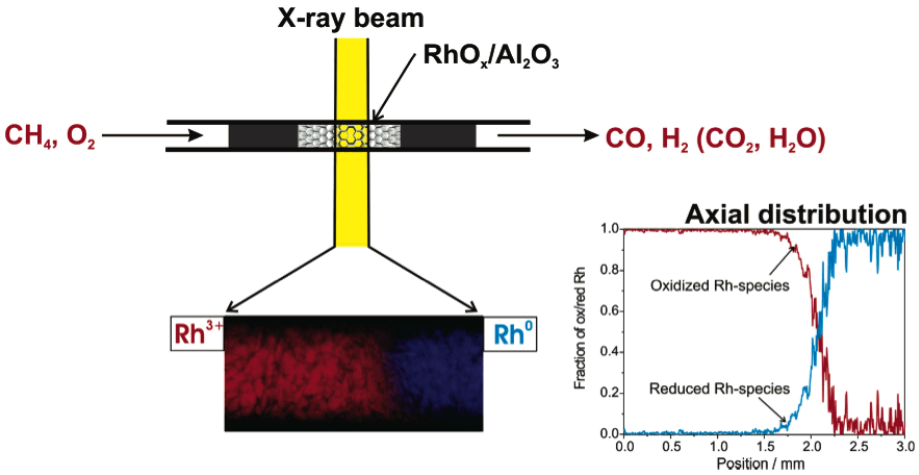

Fig. 5 Distribution of oxidized Rh-species (i.e. Rh^{3+}, red) and reduced Rh-species (i.e. Rh^0, blue) in a 10 mm long, 1.5 mm diameter fixed bed CPO reactor filled with 2.5 wt% Rh/Al_2O_3. Adopted from [39]

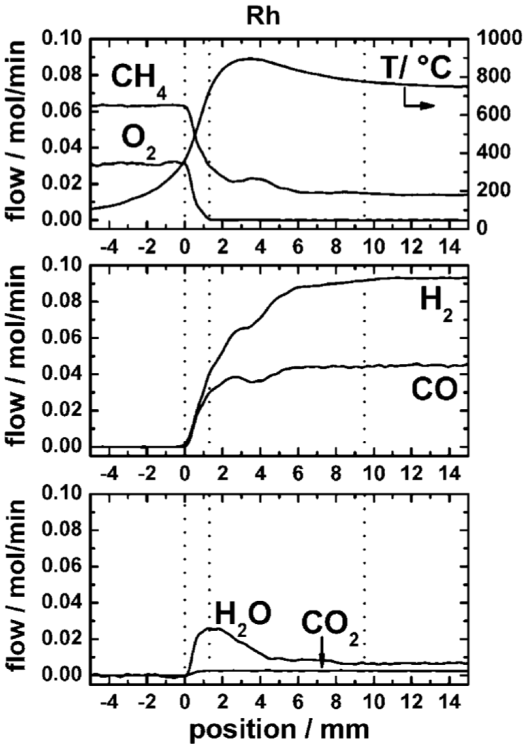

Fig. 4 Spatially resolved species and temperature profiles for methane CPO on $Rh/\alpha-Al_2O_3$ foam catalysts at $CH_4/O_2 = 2.0$ and 4.7 slpm flow rate. Adopted from [37]

of the oxygen concentration in the gas stream [39]. In the oxidation zone, Rh is in the oxidation state Rh^{3+} but becomes gradually reduced with decreasing O_2 concentration and increasing H_2 concentration to Rh metal. Kinetic studies render difficult because methane CPO is extremely fast and mass and heat transfer artifacts can hardly be eliminated. As reviewed by Enger [36] no unified mechanistic picture for methane CPO could be formulated yet. On selected systems, such as Rh [40, 41] and Pt [42,43], very detailed elementary step microkinetic models were postulated based on hierarchical multiscale modeling. On Rh, model predictions are in excellent agreement with experimental data [38,41,44]. On Pt, agreement between elementary step models and experimental data is less good [45] mainly due to deactivation of Pt by coking at low oxygen partial pressure being not yet included in the kinetic model.

What are the challenges in future CPO research? In industrial reality methane CPO would have to be conducted at pressures between about 20 bar for downstream FT-synthesis and 50 bar for downstream methanol synthesis. The safe premixing of O_2 and CH_4 at elevated pressure remains a safety issue. Pure O_2 is the preferred oxidant for methane CPO but air separation is costly. Hence integrated O_2/N_2 separation, e.g. by membranes would be highly desirable[46]. From the catalyst perspective, temperature and coke resistant CPO catalysts are required. Pt nanoparticles embedded in a high temperature stabilized barium hexaaluminate support [47] or nobel metal free catalysts such as $Co/Ca/Al_2O_3$ [48] are interesting developments.

4 Direct Conversion of Methane to Chemicals

Chapter 3 summarized status quo and research challenges in catalytic conversion of methane to synthesis gas. Now we focus on direct conversion pathways of methane to chemicals such as hydrogen cyanide, ethylene, methanol, formaldehyde, methyl chloride, methyl bromide and benzene. Compared to syngas production, direct methane conversion processes are, with the exception of HCN synthesis, still at the research stage.

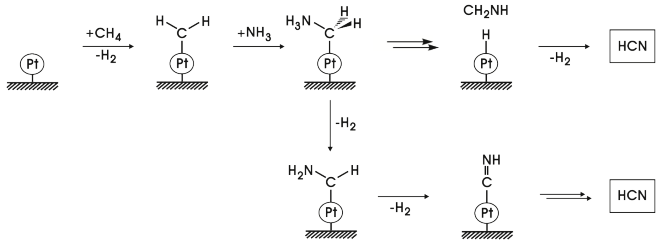

Fig. 6 Mechanism for the platinum-catalyzed methane/ammonia coupling proposed by Schwarz et al. [49]. Adopted from [49]

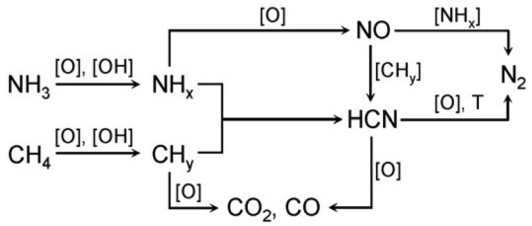

Fig. 7 Reaction network of the Andrussow process on a Pt-Rh gauze catalyst proposed by Kondratenko [53] based on TAP and isotope labeling experiments. Adopted from [53]

4.1 Methane to Hydrogen Cyanide

Hydrogen cyanide is formed from methane and ammonia in absence of oxygen (BMA-process, Eq. 17) or in presence of oxygen (Andrussow-process, Eq. 18).

$$\mathrm{CH_4(g) + NH_3(g) \rightarrow HCN(g) + 3H_2(g)} \quad (17)$$

$$\Delta H_r^\circ(298\ \mathrm{K}) = +251\ \mathrm{kJ \cdot mol^{-1}}$$

$$\mathrm{CH_4(g) + NH_3(g) + 3/2O_2(g) \rightarrow HCN(g) + 3H_2O(g)} \quad (18)$$

$$\Delta H_r^\circ(298\ \mathrm{K}) = -481\ \mathrm{kJ \cdot mol^{-1}}$$

The endothermic BMA process is conducted in externally fired tubular reactors at about 1200 °C with a Pt catalyst coated to the tube wall. The exothermic Andrussow process uses adiabatic catalytic gauze reactors (Pt/Rh gauzes) at millisecond contact times. Both, the BMA- and the Andrussow process are industrially established processes conducted essentially unchanged since decades. Compared to syngas formation relatively little fundamental or applied research has been devoted to HCN synthesis.

Much atomistic insight on the BMA process came from the work of Schwarz et al. [49]. By combining experiments in a Fourier Transform Ion Cyclotron Resonance (FTICR) mass spectrometer and B3LYP calculations on the reaction of methane and ammonia with Pt^+ ions as model catalyst in the gas-phase, Schwarz et al. identified two reaction sequences (Fig. 6) in which HCN is formed. The upper sequence involves dehydrogenation of the intermediate methanimine $H_2C = NH \rightarrow HCN + H_2$ in the gas-phase, an almost thermoneutral reaction. The lower sequence is purely catalytic. In an experimental study by Horn et al. [50] in which the reacting gases in a model BMA reactor were quenched and analyzed by molecular beam mass spectrometry and threshold ionization, $H_2C{=}NH$ was indeed detected in the gas-phase supporting the dehydrogenation step proposed earlier by Schwarz et al. [49]. To which extent the upper and lower HCN formation sequences in Fig. 6 contribute to the overall HCN formation rate remains to be studied.

A different HCN formation pathway in the BMA-process was suggested by Schuurman et al. [51] based on TAP experiments. They observed a rapid HCN formation upon admitting a CH_4 pulse 0.8 s after an NH_3 pulse and a slow HCN formation if NH_3 was pulsed 0.8 s later than CH_4. From this and other TAP experiments Schuurman et al. [51] concluded that CH_4 adsorbs and dissociates rapidly on Pt while NH_3 dissociation is slow. They suggest that HCN formation occurs through the following pathways:

$$\mathrm{N^* + CH^* \rightarrow HCN(g) + 2*} \quad (19)$$

$$\mathrm{CN^* + H^* \rightarrow HCN(g) + 2*} \quad (20)$$

Platinum remains the best catalyst for the BMA process to date. However, high throughput experimentation combined with genetic algorithm, analysis of variance and regression trees revealed that additives such as Ir, Au, Ni and Re and also alternative supports such as Si_3N_4 or SiC have a positive effect on the HCN yield [52].

Addition of oxygen to a CH_4/NH_3 feed enhances HCN formation rate by several orders of magnitude. Hence the Andrussow-Process uses adiabatically operated catalytic gauze reactors with Pt/Rh gauzes as catalyst. TAP experiments in combination with isotope labeling provided interesting insight into the reaction network of the Andrussow process [53] which are summarized in Figure 7. On the practical side, the result of Schmidt et al. [54] is important, showing that H_2 addition increases the HCN selectivity from 74 to 82 % in the Andrussow Process. Because H_2 is formed as a side product in the Andrussow process, a recycle would be sufficient. H_2 acts as sacrificial fuel reducing NH_3 conversion and N_2 formation.

4.2 Methane Oxidative Coupling (OCM)

OCM with Dioxygen The direct conversion of methane to ethylene would be of high industrial interest. In the

early 1980s, Keller and Bhasin [55] as well as Hinsen and Baerns [56] reported that ethylene is formed from methane and oxygen on a variety of metal oxide catalysts at temperatures between 500 − 1000 °C. The reaction, called Oxidative Coupling of Methane (OCM), is shown in Eq. 21.

$$\mathrm{CH_4(g) + 1/2O_2(g) \rightarrow 1/2C_2H_4(g) + H_2O(g)} \qquad (21)$$
$$\Delta H_r^\circ(1073\ \mathrm{K}) = -139\ \mathrm{kJ \cdot mol^{-1}}$$

Since this pioneering work OCM has been studied intensely. Zavyalova and Baerns [57] reviewed the vast OCM literature in 2011 and reported more than 2700 research articles and about 140 patents at that time. Already in 1993 Maitra reviewed global performance data of OCM catalysts and identified those for which the sum of methane conversion and C_{2+} selectivitiy was higher than 80 % at more than 5 % CH_4 conversion [58]. Maitra listed 283 chemically vastly different materials overcoming this limit. The only thing they have in common is that all were oxides.

Despite intense research, no industrial process resulted so far. Only recently, a San-Francisco based start-up company called Siluria Technologies announced the completion of an OCM demonstration plant in foreseeable future using novel nanowire catalysts [59]. According to Siluria, the technology would be superior to naphtha reforming, the conventional technology for ethylene production. However, no performance data or any further information about the catalyst was revealed.

The most severe technological barrier in terms of process development is the insufficient selectivity of all tested OCM catalysts at industrially relevant conversion levels. Figure 8 shows X, S-data of the best OCM catalysts reported in literature that were scrutinized by Zavyalova and Baerns [57] for being measured in kinetically sound experiments. These data indicate that C_2 selectivity ($C_2H_4 + C_2H_6$) decreases with increasing CH_4 conversion resulting in a virtual one pass yield limit between 25 % and 30 %. Indeed an inherent yield barrier of about 30 % was predicted by Labinger already in 1988 [60] based on kinetic arguments that radical H· abstraction is insensitive to the nature of the hydrocarbon molecule. Hence, not only CH_4 but also the coupling products C_2H_6 and C_2H_4 are activated on the catalyst leading to decreasing selectivity at increasing conversion.

Mechanistically OCM is discussed as a 'heterogeneous-homogeneous' reaction. This mechanistic pictures was based on the detection of CH_3· radicals over Li/MgO and Sr/La_2O_3 OCM catalysts during reaction by EPR-spectroscopy [61,62] or molecular beam mass spectrometry [63,64]. An apparent correlation between the Li

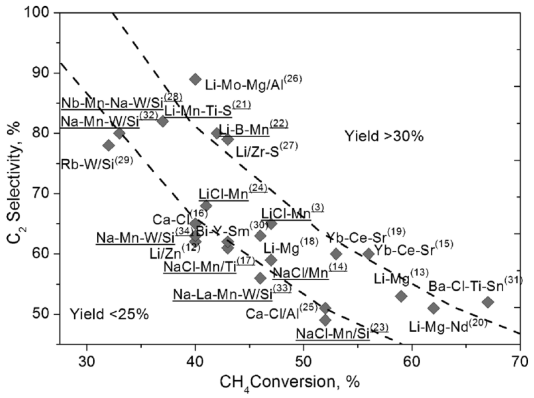

Fig. 8 Elemental compositions of OCM catalysts with $Y(C_2) \geq 25$ % reported in the literature. All catalysts were tested in a fixed-bed reactor in a co-feed mode under atmospheric pressure at temperatures from 943 K to 1223 K, $p(CH_4)/p(O_2) = 1.7 - 9.0$, and contact times from 0.2 to 5.5 s. Figure adapted from [57].

concentration in Li/MgO catalysts, the C_2 productivity and the CH_3· productivity was observed [65] leading to the conclusion that the Li/MgO catalyst released CH_3· radicals to the gas-phase where they couple to C_2H_6, the primary coupling product. Li^+O^- sites were thought to be the active centers without that there exists any proof in literature that these sites exist under OCM reaction conditions.

Recently, OCM research has gained momentum again. Li/MgO was reviewed [66] and studied again in great detail but neither experiment nor theory gave evidence that Li^+O^- exists under OCM conditions [67]. Both on a Li-doped MgO film grown on a Mo(001) substrate but also on Li-doped MgO powders surface segregation of Li was observed above 700 K and Li-desorption above 1050 K. Fig. 9 shows the surface of such a Li-doped MgO-film upon heating to 700 K and 1050 K. The formation of Li-rich surface oxides patches and the rectangular surface defects left behind upon Li-desorption are clearly seen and in line with ab-intio thermodynamic calculations [67]. It can be summarized that Li-doping leads to a pronounced morphology change and defect formation on the MgO surface which has a positive effect on the OCM activity. However, the initially high OCM activity cannot be sustained due to Li-losses under reaction conditions rendering Li/MgO and also other Li-based OCM catalysts unusable for process development.

The identity of the active site for methane activation on OCM catalysts remains open. According to Schwarz [68], oxygen centered radicals on metal oxides are active for homolytic hydrogen abstraction from methane (Eq. 22).

$$\mathrm{MO \cdot + H - CH_3 \rightarrow MO - H + CH_3 \cdot} \qquad (22)$$

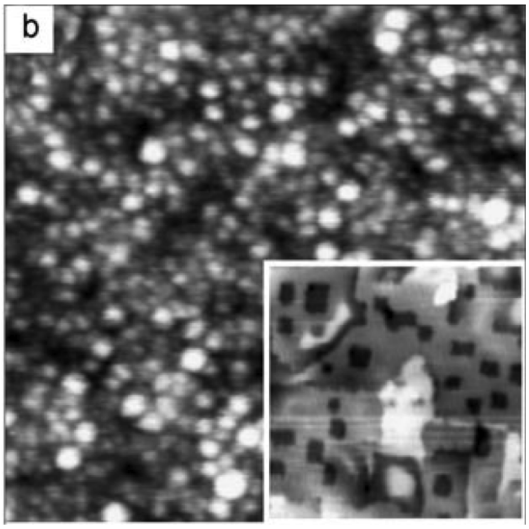

Fig. 9 STM image of a 12 ML thick oxide film prepared by co-depositing Li and Mg in an O_2 ambience after annealing to 700 K and 1050 K (inset). Figure adapted from [67].

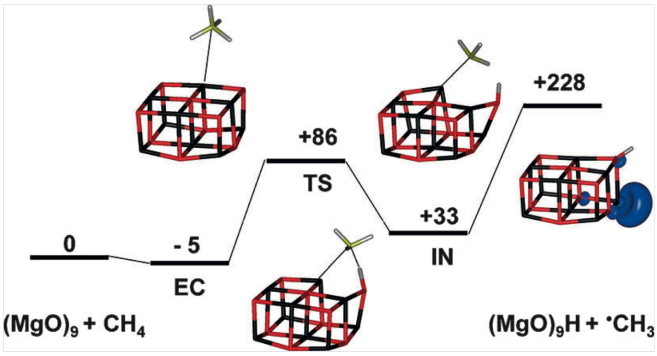

Fig. 10 Reaction energy diagram for chemisorption of CH_4 onto corner/edge sites of a Mg_9O_9 cluster showing C–H bond addition on an $Mg^{2+}O^{2-}$ pair. B3LYP energies in $kJ \cdot mol^{-1}$. Figure adapted from [69].

This mode of methane activation would be in line with the $\left[Li^+O^-\right]_{MgO}$ site postulated by Lunsford et al. [65]. On the other hand, recent calculations by Sauer et al. [69] show that $\left[Li^+O^-\right]_{MgO}$ sites would be overly reactive for homolytic C–H cleavage with an activation barrier as low as $27 \pm 7\ kJ \cdot mol^{-1}$. Instead the calculation results point to an alternative methane activation pathway on steps and corners of MgO shown in Fig. 10 and summarized by Equation 23.

$$\left[Mg^{2+}O^{2-}\right]_{MgO} + H - CH_3 \rightarrow \left[HO^-(Mg - CH_3)^+\right]_{MgO} \quad (23)$$

$CH_3\cdot$ radical desorption requires 228 $kJ \cdot mol^{-1}$ and would be, without any coreactant, hardly feasible (Fig. 10). However, the unpaired electron formed in this reaction on the magnesium ion could facilitate O_2 chemisorption as a superoxide species in a very exothermic reaction ($-191\ kJ \cdot mol^{-1}$, Eq. 24) such that the overall reaction (Eq. 25) would become almost thermoneutral.

$$\left[HO^-(Mg^{\cdot -})+\right]_{MgO} + O_2 \rightarrow \left(O_2^{\cdot -}\right)\left[HO^-Mg^{2+}\right]_{MgO} \quad (24)$$

$$\left[Mg^{2+}O^{2-}\right]_{MgO} + CH_4 + O_2 \rightarrow \left(O_2^{\cdot -}\right)\left[HO^-Mg^{2+}\right]_{MgO} + CH_3\cdot \quad (25)$$

If one of these, both or another mechanism is responsible for methane activation remains subject to further studies including also more complex catalysts than Li/MgO such as $Na_2WO_4/Mn/SiO_2$ for example. The involvement of $CH_3\cdot$ radicals seems certain because labeling experiments with CH_4/CD_4 mixtures led exclusively to symmetrically substituted coupling products C_2H_6, CD_3CH_3, C_2D_6, C_2H_4, CH_2CD_2 and C_2D_4[70]. However, whether this coupling step occurs in the gas-phase or at the catalyst surface cannot be concluded from this product pattern and also not from the mere detection of gas-phase $CH_3\cdot$ radicals. In fact, the coupling of two $CH_3\cdot$ radicals in the gas-phase is a rather inefficient step because a third collision partner is required to carry away the excess energy $CH_3 \cdot + CH_3 \cdot + M \rightarrow C_2H_6 + M^*$ while the gas-phase oxidation steps of $CH_3\cdot$ radicals to HCHO forming finally H_2 and CO are bimolecular, e.g. $CH_3 \cdot + \cdot O_2H \rightarrow CH_3O \cdot + OH\cdot$, and hence much more efficient. Detailed microkinetic simulations combining surface and gas-phase reaction steps will be necessary to explore the heterogeneous-homogeneous nature of OCM further. However, without sound knowledge of the active center, surface elementary steps, activation barriers and rate constants, such simulations are of little value.

OCM with Sulfur From a thermodynamic point of view, O_2 is a very strong oxidant and the driving force for methane overoxidation to CO or CO_2 is high. Following this line of thought, Neurock and Marks [71] proposed elemental sulfur as a 'softer' oxidant for selective methane conversion to ethylene. As summarized in Fig. 11, the oxidation of methane to ethylene by elemental sulfur is thermodynamically feasible at high temperatures, e.g. 1073 K, but the driving force for total oxidation to CS_2 is considerably reduced. Transition metal sulfides like MoS_2, RuS_2, TiS_2 and PbS, known as desulfurization catalysts in the petrochemical industry, showed activity and selectivity for sulfur mediated coupling of methane to ethylene. Ab initio DFT calculations showed that all transition metal surfaces were highly sulfided under experimental conditions (5 % CH_4 in Ar, $CH_4/S = 5.8$) and that the active sites comprised S–S pairs [71]. A linear but inverse relation between the metal-sulfur bond strength, the rate of methane

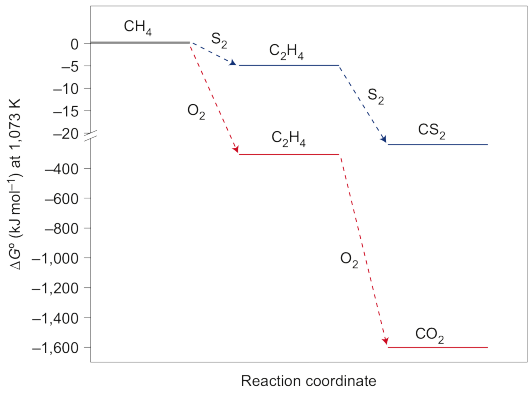

Fig. 11 Gibbs free energy changes for methane oxidation by S_2 (red) and O_2 (blue) to C_2H_4 and further to CS_2 and CO_2 respectively. Figure taken from [71].

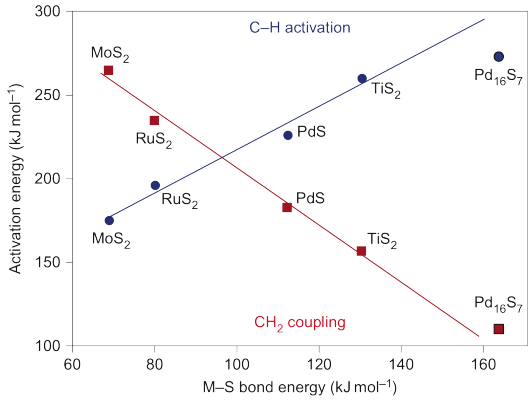

Fig. 12 DFT calculated activation barriers for methane C–H activation (blue) and the coupling of methylene intermediates (CH_2–S*, red) as a function of the M–S bond strenght. Figure taken from [71].

activation (CH_4 conversion) and the rate of CH_2 coupling (C_2H_4 selectivity) was found (Fig. 12). The DFT results in Fig. 12 suggest that PbS seems to make a good compromise between activity and selectivity and indeed, among the four sulfides tested, PbS showed the best performance with about 15.3 % CH_4 conversion and 18.2 % C_2H_4 selectivity. Off course, these value are very low are and far beyond any commercial interest. Nevertheless, methane oxidative coupling to ethylene using sulfur as soft oxidant is an interesting strategy that should be followed on in the future.

4.3 Methane Oxidation to Methanol and Formaldehyde

The direct oxidation of methane to methanol (Eq. 26) and/or formaldehyde (Eq. 27) are 'dream reactions' for heterogeneous catalysis but despite decades of research, both are even further away from practical application than OCM.

$$\mathrm{CH_4(g) + 1/2O_2(g) \rightarrow CH_3OH(g)} \quad (26)$$
$$\Delta H_r^\circ(298\ \mathrm{K}) = -126\ \mathrm{kJ \cdot mol^{-1}}$$
$$\mathrm{CH_4(g) + O_2(g) \rightarrow CH_2O(g) + H_2O(g)} \quad (27)$$
$$\Delta H_r^\circ(298\ \mathrm{K}) = -368\ \mathrm{kJ \cdot mol^{-1}}$$

Nature is far ahead of chemists and catalysis researchers for methanotrophic bacteria utilize methane as carbon and energy source with methane oxidation to methanol being the first step in their metabolism [72].

There is little hope that high temperature heterogeneous catalytic pathways will ever lead to acceptable methanol or formaldehyde yields because, as pointed out by Labinger [73], high temperature methane oxidation is a consecutive reaction ($A \xrightarrow{k_1} B \xrightarrow{k_2} C$) proceeding via homolytic C–H bond cleavage. As the C–H bond strength in H–CH_2OH (≈ 95 kcal $\cdot$ mol^{-1}) and in H–CHO (≈ 87 kcal $\cdot$ mol^{-1}) is lower than in H–CH_3 (≈ 105 kcal$\cdot$mol^{-1}), k_2 will be larger than k_1 (typically $k_2/k_1 > 20$) and methanol or formaldehyde yields will be a few percent at best.

Methane Oxidation to Formaldehyde As reviewed by Vekki and Marakaev [74], the results for gas-phase methane oxidation to formaldehyde on classical heterogeneous oxidation catalysts are uninspiring from an application point of view. MoO_x/SiO_2 and VO_x/SiO_2 are among the most thoroughly studied catalysts but formaldehyde yields are on the order of 3 – 4 % at best. It is difficult to assess the catalytic performance of MoO_x/SiO_2 and VO_x/SiO_2 catalysts and to establish structure activity correlations because i) the SiO_2 support shows nearly the same activity/selectivity pattern for methane oxidation to formaldehyde [75] and because ii) gas-phase reactions occur in parallel to catalytic surface reactions [76].

Higher HCHO space time yields than on precipitated silica are obtained if mesoporous silica is used as support such as in VO_x/MCM-41 [77,78], VO_x/MCM-48 [77], VO_x/SBA-15 [79], CuO_x/SBA-15 [80] and FeO_x/SBA-15 [81]. Isolated monomeric transition metal oxide species, short residence times and the addition of steam have a positive effect on formaldehyde selectivity. Nevertheless, also on mesoporous catalysts the one pass yields to formaldehyde are on the order of 3 %. Even with engineering 'tricks' such as formaldehyde quenching by water film adsorption on cooled reactor parts [82, 83] or reactant recycle [84] these values are still too low for process development.

Modern experimental and theoretical methods provide molecular insight into methane activation on silica

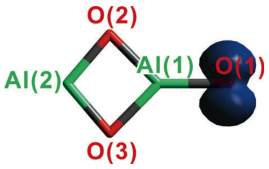

Fig. 13 Optimized ground-state structure of $[Al_2O_3]^{\cdot+}$ (C2v) as revealed by DFT calculations; the blue isosurface indicates the spin-density distribution. Figure taken from [86].

supported transition metal oxides providing an explanation of unsatisfactory performance of these materials on the one hand and pointing out more promising research directions on the other hand. DFT calculations and mass spectrometric experiments reacting CH_4 with $V_xSi_yO_z^+$ cluster ions in the gas-phase [85] show that these cluster ions possess a terminal oxygen centered radical $O_t^{\cdot}$ activating methane by homolytic bond cleavage and releasing a methyl radical into the gas-phase (Eq. 28).

$$[(V_2O_5)_n(SiO_2)_m]^+ + CH_4 \rightarrow [(V_2O_5)_n(SiO_2)_mH]^+ + CH_3\cdot \quad (28)$$
$$(n = 1, m = 1-4; n = 2, m = 0, 1)$$

If Eq. (28) is the mode of methane activation on supported VO_x/SiO_2 catalysts the low one pass formaldehyde yields could be the consequence of unselective consecutive reactions of the generated $CH_3\cdot$ radicals in the gas-phase.

An alternative and possibly more promising reaction channel was reported by Schwarz et al. [86]. Again by using a combination of mass spectrometric experiments and DFT calculations on reactions of CH_4 with gas-phase metal oxide cluster ions, the $[Al_2O_3]^{\cdot+}$ cation (Fig. 13) was found to react with methane in two competing reaction channels (Eq. 29, 30):

$$[(Al_2O_3)]^{\cdot+} + CH_4 \rightarrow [(Al_2O_3H)]^+ + CH_3\cdot (35\ \%) \quad (29)$$

$$[(Al_2O_3)]^{\cdot+} + CH_4 \rightarrow [(Al_2O_2H_2)]^{\cdot+} + CH_2O (65\ \%) \quad (30)$$

Reaction (29) liberates $CH_3\cdot$ radicals just like the terminal oxygen centered radicals in Reaction (28). As discussed above, this pathway will result in low formaldehyde selectivity due to unselective gas-phase radical reactions. Reaction (30) on the other hand liberates CH_2O directly and because it is energetically favored ($\Delta E(30) = -2.34$ eV vs. $\Delta E(29) = -1.03$ eV) the branching ratio is 65 % to 35 % respectively. There are no results yet how the catalytic cycle will be closed and whether this reaction channel will also function on neutral supported Al_2O_3 clusters and on real catalysts but this work might stimulate further research on the selective one-step oxidation of methane to formaldehyde.

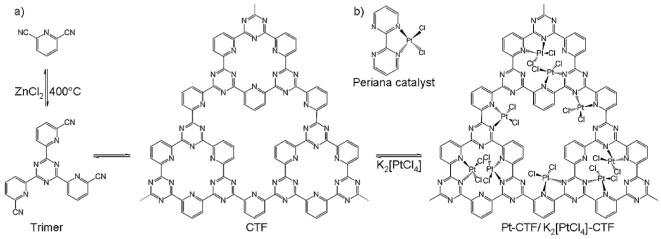

Fig. 14 a) Trimerization of $2,6-$dicyanopyridine (DCP) in molten $ZnCl_2$, conversion to a covalent triazine-based framework (CTF), and subsequent platinum coordination (Pt-CTF); b) Periana's platinum bipyrimidine complex. Figure adapted from [91].

Methane Oxidation to Methanol Compared to methane oxidation to formaldehyde, much more progress has been made in recent years in selectively oxidizing methane to methanol. The most promising heterogeneous catalytic approaches today copy concepts from homogeneous or biocatalysis. A variety of homogeneous metal complexes exist, that cleave the C–H bonds of methane and other hydrocarbons at low temperatures and with high selectivity. A detailed account on this kind of chemistry is given in the reviews by Shilov [87] and Periana [88]. As outlined in Section 2, the activation of the C–H bond of methane by strong electrophiles is probably the most facile and controllable way of methane activation. Indeed, Periana showed that polarizable ('soft') strong electrophiles such as $[XHg^+]$ ions in strongly acidic solvents like sulfuric acid react readily with methane via C–H activation at temperatures below 200 °C [88]. At 180 °C with a 20 mM concentration of $Hg(HSO_4)_2$ in sulfuric acid methanol yields of over 40 % at $>$ 90 % selectivity were obtained (Eq. 31) [88,89].

$$CH_4 + H_2SO_4 \xrightarrow{Hg(II)/H_2SO_4} CH_3OH + H_2O + SO_2 \quad (31)$$

Later, Periana [90] reported a Pt-based catalyst, Dichloro($\eta-2-[2,2'-$bipyrimidyl])platinum(II)[(bpym)$PtCl_2$], which gave 90 % methane conversion at 81 % selectivity to methyl bisulfate which can be hydrolyzed to methanol and sulfuric acid.

Palkovits et al. [91] used Periana's molecular template and developed a covalent triazine-based framework (CTF) by trimerization of 2,6-dicyanopyridine in molten $ZnCl_2$. This solid ligand coordinates $PtCl_2$ forming a solid analog to Periana's (bpym)$PtCl_2$ system (Fig. 14). Indeed, the Pt-CTF is active in methane oxidation in oleum to methyl-bisulfate which, after workup,

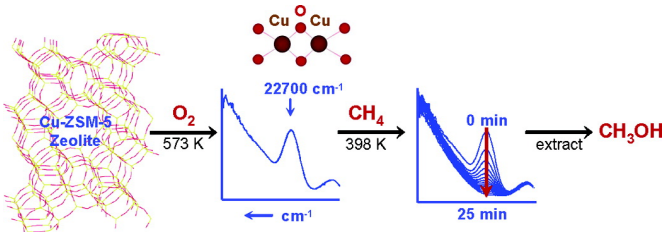

Fig. 15 Fiber-optic UV-vis spectra of O_2-activated Cu-ZSM-5 with Si/Al=12 and Cu/Al=0.58 during reaction with CH_4. Figure taken from [94].

gives methanol. The catalyst undergoes an activation period but eventually reaches TONs above 250. The work of Palkovits et al. [91] is an example of a low temperature heterogeneously catalyzed methane oxidation pathway. It illustrates nicely how heterogeneous catalysis can benefit from concepts of homogeneous catalysis. Certainly, for methane oxidation at an industrial scale, the space time yield of this batch process is much too low and the workup of the intermediate methylbisulfate and the re-oxidation of SO_2 might be prohibitively expensive. Another problem was that about 5−10 wt% of the CTF-Pt catalyst was lost in each recycling step. Nevertheless, it is a first example of a heterogeneous low temperature methane oxidation pathway with a technologically relevant yield.

A second interesting low temperature methane oxidation pathway is that on zeolite catalysts containing transition metal ions [92], in particular Cu, Fe and Co. The extra-framework transition metal ions decompose NO and N_2O but also activate O_2 as oxidant. ZSM-5 is the most prominent host lattice but other zeolites have been used as well. On Cu-ZSM-5, one of the most thoroughly studied systems, UV-Vis, EPR and EXAFS indicate that a Bis-(μ-oxo)dicopper(III) core, i.e. $[Cu_2(\mu\text{-}O)_2]^{2+}$, is formed upon reaction with NO [93]. This site, most conveniently followed by the UV-Vis absorption band at 22700 cm^{-1}, disappears on reaction with CH_4 already at 398 K and methanol can be extracted with a 1:1 water/acetonitrile mixture (Fig. 15). In later studies, resonance Raman spectroscopy, $^{18}O_2$ oxygen labeling, DFT and normal coordinate analysis was used to refine the active center to be a bent mono-(μ-oxo)dicupric site $[Cu_2O]^{2+}$[95]. Recently Quick X-ray Absorption Spectroscopy was used to follow the electronic and structural changes to the active Cu sites in Cu-MOR during reaction with methane and desorption of methanol [96]. It was found that the structure of the active Cu-site was a function of the reaction conditions as summarized in Figure 16. In a dry environment, the already known mono-(μ-oxo)-dicopper(II) site activates CH_4. CO_2 or CH_3OH are released upon heating in absence or presence of H_2O. In a moist oxidation environment, a water stable Cu^{II}-oxide species is responsible for CH_4 activation.

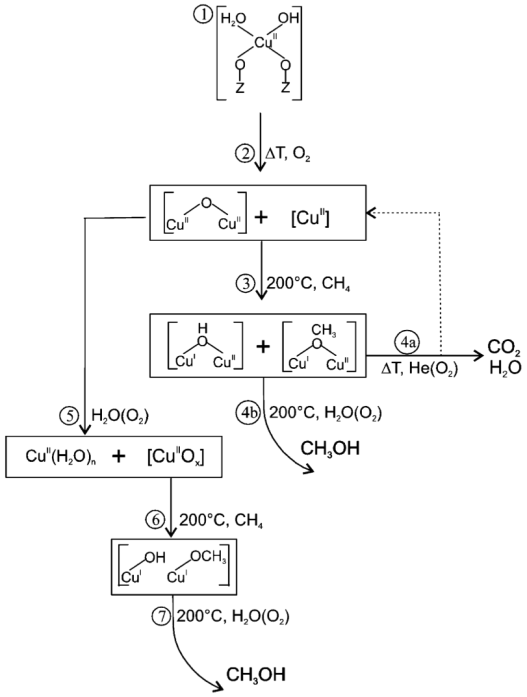

Fig. 16 Methane activation and product desorption as function of reaction conditions on a $Cu-MOR$ catalyst. Figure taken from [96].

4.4 Methane Halogenation and Oxy-Halogenation

Methane reacts with all halogens to halogenated products. For a large scale process, only the reactions with chlorine Eq. (32) and with bromine Eq. (33) are of practical interest.

$$CH_4(g) + Cl_2(g) \rightarrow CH_3Cl(g) + HCl(g) \qquad (32)$$
$$\Delta H_r^\circ(298\ \mathrm{K}) = -99.6\ \mathrm{kJ \cdot mol^{-1}}$$
$$CH_4(g) + Br_2(g) \rightarrow CH_3Br(g) + HBr(g) \qquad (33)$$
$$\Delta H_r^\circ(298\ \mathrm{K}) = -28.0\ \mathrm{kJ \cdot mol^{-1}}$$

Fluorine is too reactive, corrosive and toxic while the reaction of methane with iodine is thermodynamically constrained and methyl iodide decomposes at elevated temperatures. Alternatively, methane reacts with HBr and O_2 to CH_3Br, a reaction called oxy-bromination (OBM, Eq. 34). The reaction of methane with HCl and O_2, called oxy-chlorination, is likewise feasible.

$$2CH_4(g) + 2O_2(g) + HBr(g) \rightarrow$$
$$CH_3Br(g) + CO(g) + 3H_2O(g) \qquad (34)$$
$$\Delta H_r^\circ(298\ \mathrm{K}) = -686\ \mathrm{kJ \cdot mol^{-1}}$$

Methyl chloride and methyl bromide are valuable intermediates which can be converted to olefines, alcohols, aromatics, ethers or liquid hydrocarbons (Eq. 35-37, X=Cl,Br).

$$CH_3X + H_2O(g) \rightarrow CH_3OH + HX \quad (35)$$

$$CH_3X + CH_3OH \rightarrow CH_3OCH_3 + HX \quad (36)$$

$$2CH_3X \rightarrow CH_2CH_2 + 2HX \quad (37)$$

In oxy-bromination of methane a mixture of CH_3Br, CO and H_2O forms, which can be converted to acetic acid.

$$CH_3Br(g) + CO(g) + H_2O(g) \rightarrow CH_3COOH(g) + HBr(g) \quad (38)$$

$$\Delta H_r^\circ(298\ \mathrm{K}) = -89\ \mathrm{kJ \cdot mol^{-1}}$$

In each case, HBr and HCl are liberated and could be recycled.

All halogenation and oxy-halogenation reactions mentioned above can be conducted on heterogeneous catalysts at temperatures between $450 - 650$ °C. For example, methane-oxychlorination is catalyzed by LaOCl or $LaCl_3$ [97]. Selective bromination of methane to methyl bromide is possible on SO_4^{2-}/ZrO_2 modified SBA-15 catalysts [98]. A catalyst with 25 wt% SO_4^{2-}/ZrO_2 showed 99 % selectivity to CH_3Br at 69 % CH_4 conversion. The selective formation of CH_3Br is very important because CH_2Br_2 leads to coking in subsequent reactions. Methane oxy-bromination (Eq. 34) is catalyzed by Ru/SiO_2 [99], Rh/SiO_2 [100] or noble-metal free supported metal-oxide catalysts MO_x/SiO_2 with M being Mo, Ba or W [101]. On BaO/SiO_2, a methane conversion of 44 % at a combined selectivity of 95 % to CH_3Br, CH_3OH and CO was obtained for about 25 h time on stream [101]. $FePO_4/SiO_2$ was found to be even more active and selective for methane oxy-bromination ($X(CH_4) \approx 50$ %, $S(CH_3Br{+}CO) > 95$ %, $CH_3Br/CO \approx 1$) and showed no signs of deactivation during 200 h time on stream [102]. At similar performance, hydrothermally synthesized $FePO_4$-SBA-15 was stable for even 1000 h time on stream [103]. Recently, Ding et al. [104] studied the very rich solid state chemistry on bulk model iron phosphate catalysts using XRD, Mössbauer spectroscopy and temperature programmed reduction. By chance they discovered that the fluoride based synthesis route they applied led to formation of a $Na_3Fe_2(PO_4)_3$ phase which showed even a better catalytic performance than the $FePO_4$ phases tested before.

In summary, heterogeneous catalysts can be used to convert methane selectively to methyl chloride and methyl bromide which can, again by using solid catylsts, be transformed into valuable chemicals such as olefines, aromatics, ethers, alcohols and liquid hydrocarbons. However, compared to syngas based processes, all potential methane conversion processes based on halogenation or oxy-halogenation will have to meet the challenges of the toxicity and high corrosiveness of the chemicals involved. There is also no real cost advantage in substituting established syngas based technology for halogenation or oxy-halogenation routes because they are also multistep processes requiring expensive feed preparation, reactors and seperation units for each single step.

4.5 Methane Aromatization

The oxidative methane conversion routes discussed in the preceding Sections 4.2-4.4 are thermodynamically feasible but suffer from low selectivities to the target molecules because of overoxidation. An alternative approach for methane conversion is using no oxidant at all or lowering the oxidation potential of the feed mixture by distributed oxygen supply or milder oxidants. Representative of this strategy is the heterogeneous catalytic conversion of methane to a mixture of aromatics like benzene, naphthalene, toluene, xylenes etc. summarized by the term 'methane aromatization' (MA). Details on this reaction can be found in reviews by Ismagilov [105], Bao [106] or Spivey and Hutchings [107]. A thermodynamic analysis of methane aromatization with and without coke removing agents like H_2O, CO and CO_2 can be found in Ref. [108]. As illustrated by Eq. 39, nonoxidative methane aromatization has severe thermodynamic constraints.

$$6CH_4(g) \rightleftarrows C_6H_6(g) + 9H_2(g) \quad (39)$$

$$\Delta H_r^\circ(298\ \mathrm{K}) = +532\ \mathrm{kJ \cdot mol^{-1}}$$

$$\Delta G_r^\circ(298\ \mathrm{K}) = +434\ \mathrm{kJ \cdot mol^{-1}}$$

If no solid carbon is formed at 1000 K and 1 bar pressure, $\sim$ 15 % CH_4 conversion at $\sim$ 98 % combined selectivity to benzene and naphthalene will be possible from a thermodynamic point of view [108]. In reality carbon formation is inevitable, the selectivity to aromatics is much lower and all catalysts deactivate with time on stream due to coke formation.

Zeolites doped with transition metal ions are active for MA. HZSM-5 and HMCM-22 containing Mo, W, Re or Co/Ga are among the most active and selective MA catalysts. MA catalysts are bifunctional. Methane is activated at the transition metal ions forming a C_2H_x intermediate which is subsequently aromatized at the Brønstedt acid sites of the zeolite. Molybdenum was found to be reduced to Mo_2C or MoO_xC_y. The pore structure of the zeolite induces shape selectivity. A pore network with a pore diameter close to the kinetic diameter of a benzene molecule (~ 6Å) as in ZSM-5 and

Catalysts	Reaction time (min)	Conversion of CH_4 (%)	Selectivity[a] (%)			Yields of aromatics (%)
			Benzene	Toluene	Naphthalene	
Mo/TNU-9	60	11.3	81.2	2.2	16.6	6.2
	300	9.8	89.2	1.1	9.7	5.4
Mo/ZSM-5	60	9.5	67.4	2.4	30.2	5.6
	300	6.9	78.3	1.5	20.2	4.1

[a] Without counting for coke. Reaction condition: T = 973 K, 1 atm, GHSV = 1500 h^{-1}.

Fig. 17 The reaction results of methane aromatization over Mo/TNU-9 and Mo/ZSM-5 catalysts at 60 and 300 min. Figure taken from Reference [109].

MCM-22 seems to be beneficial. Liu et al. [109] used a Mo/TNU-9 catalyst with a three-dimensional 10-ring channel system which showed even a higher benzene selectivity and more importantly a higher stability than Mo/ZSM-5 (Fig. 17).

A promising novel high temperature MA route was recently reported by Bao et al. [110]. On catalysts containing single iron sites in a silica matrix, methane could be converted to ethylene and aromatics at > 99 % selectivity. At 1363 K methane conversion peaked at 48.1 % at 48.4 % ethylene selectivity. The catalyst showed stable performance for 60 h time on stream. The reaction mechanism was postulated to comprise catalytic generation of $CH_3\cdot$ radicals followed by product formation in the gas-phase. $CH_3\cdot$ radicals were detected by vacuum ultraviolet soft photoionization molecular-beam mass spectrometry. Fe-site isolation occurred under reaction conditions and was verified by HAADF-STEM and XANES. Reaction steps from methane activation to naphthalene were rationalized by DFT-simulations.

Whether the results of Bao et al. [110] are reproducible has to be seen. The reaction products found are typical for methane pyrolysis and the absence of acetylene can be attributed to the still moderate temperature. If the reaction occurs by radical reactions in the gas-phase the question arises why it would stop at the stage of naphthalene. However, the published results are very interesting and will definitely stimulate further research.

5 Summary and Outlook

Methane activation by heterogeneous catalysis is of great importance to secure the future supply of energy, fuels and chemicals for our modern society. Aside from the vast reserves and resources of fossil methane in natural gas, methane activation is also key if biogas is to be used as chemical raw material. Due to the chemical inertness of the CH_4 molecule compared to the desired target products, very few direct, viz. one-step methane conversion processes have been realized so far. Large scale industrial methane conversion still relies on synthesis gas which can be converted to fuels and chemicals in downstream processes. No new process has been developed in the past years converting methane directly to ethylene, formaldehyde, methanol, aromatics or liquid hydrocarbons. Superficially viewed not much progress has been made in industrial methane chemistry since decades.

However, a closer look into methane activation, in particular with the aid of heterogeneous catalysts as in the present review, shows, that enormous progress has been made in terms of understanding and applying concepts of catalytic methane activation. The combination of knowledge based catalyst synthesis, advanced microscopic and spectroscopic catalyst characterization and high level computational methods brought about several important results in the quest for heterogeneous catalytic methane activation. The design of coke resistant steam reforming catalysts by selective poisoning, perovskite based precursors for coke-resistant Ni nano-particles as dry reforming catalysts, the molecular inspired design of supported electrophiles to oxidize methane to methanol or the non-oxidative conversion of methane to aromatics on single iron sites in a silica matrix are just a few examples of this successful approach.

Apart from methane conversion to synthesis gas and hydrocyanic acid, most results and developments discussed in this review are at a very early stage and far away from any industrial application. Nevertheless, the molecular details of catalytic methane activation at high and low temperatures become more and more transparent. Nature is still far ahead in methane chemistry but catalysis researchers are catching up.

References

1. BP, BP Statistical Review of World Energy June 2013. Tech. rep., BP (2013)
2. R.A. Dawe, S. Thomas, Energ. Source Part A **29**, 217 (2007)
3. Y.F. Makogon, S.A. Holditch, T.Y. Makogon, J. Petrol. Sci. Eng. **56**, 14 (2007)
4. Q. Wang, X. Chen, A.N. Jha, H. Rogers, Renew. Sus. Energ. Rev. **30**(1-28) (2014)
5. P. Weiland, Appl. Microbiol. Biotechnol. **85**, 849 (2010)
6. (2014). URL http://www.eurobserv-er.org
7. S.I. Oni, M.A. Oyewo, J. Hum. Ecol. **33**(1), 21 (2011)
8. E. Broctawik, Advances in Quantum Chemistry **33**, 349 (1998)
9. N. Dietl, M. Schlangen, H. Schwarz, Angew. Chem. Int. Ed. **51**, 5544 (2012)
10. B.R. Wood, J.A. Reimer, A.T. Bell, M.T. Janicke, K.C. Ott, J. Catal. **225**, 300 (2004)
11. URL www.ceresana.com/en/market-studies/agriculture/ammonia

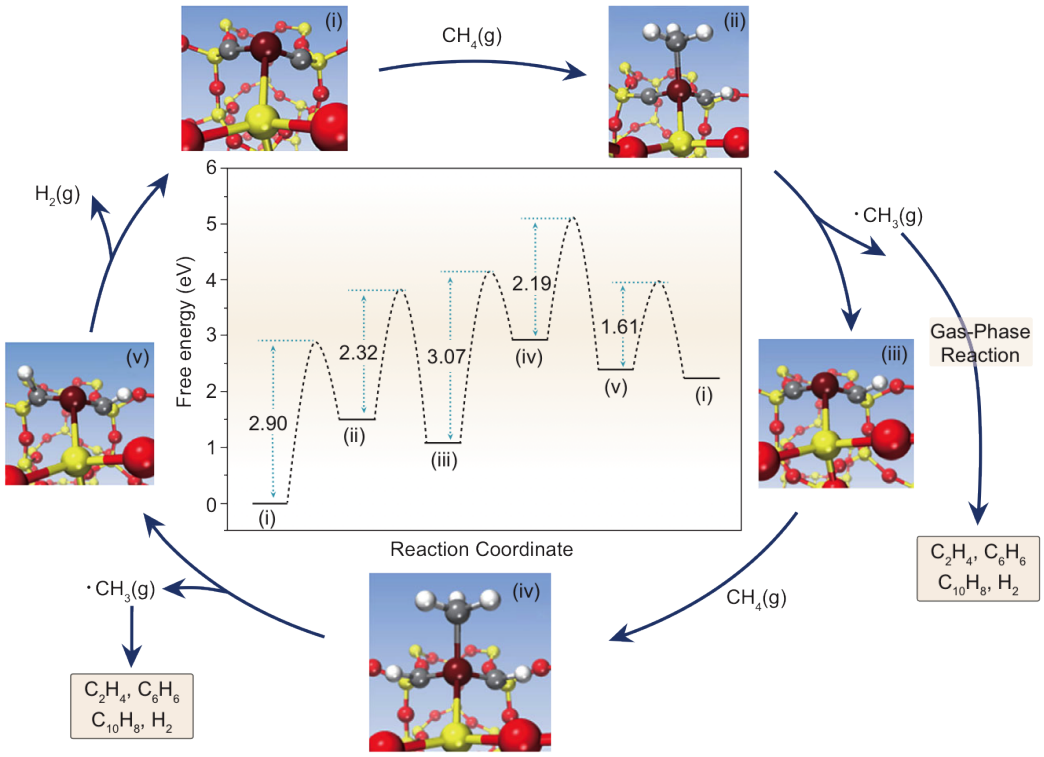

Fig. 18 Catalytic cycle and DFT-results for $2CH_4 \rightarrow 2CH_3 \cdot + H_2$ on Fe©SiO_2. Figure taken from Reference [111].

12. URL www.methanol.org/Methanol-Basics/The-Methanol-Industry.aspx
13. A. Jess, P. Wasserscheid, *Chemical Technology* (WILEY-VCH, 2013)
14. K. Aasberg-Petersen, I. Dybkjaer, C.V. Ovesen, N.C. Schjodt, J. Sehested, S.G. Thomson, J. Nat. Gas Sci. Eng. **3**, 423 (2011)
15. J.R. Rostrup-Nielsen, J. Sehested, J.K. Norskov, Adv. Catal. **47**, 65 (2002)
16. J.N. Armor, Appl. Catal. A Gen. **176**, 159 (1999)
17. J.R. Rostrup-Nielsen, L.J. Christiansen, *Concepts in Syngas Manufacture*, *Catalytic Science Series*, vol. 10 (Imperial College Press, 2011)
18. K. Lu, C. Song, V. Subramani (eds.), *Hydrogen and Syngas Production and Purification Technologies* (John Wiley and Sons, Inc., 2010)
19. G. Jones, J.G. Jakobsen, S.S. Shim, J. Kleis, M.P. Andersson, J. Rossmeisl, F. Abild-Pedersen, T. Bligaard, S. Helveg, B. Hinnemann, J.R. Rostrup-Nielsen, I. Chorkendorff, J. Sehested, J.K. Norskov, J. Catal. **259**(147) (2008)
20. J. Wei, E. Iglesia, J. Catal. **224**, 370 (2004)
21. J. Sehested, Catal. Today **111**, 103 (2006)
22. J. Sehested, N.W. Larsen, H. Falsig, B. Hinnemann, Catal. Today **228**, 22 (2014)
23. H.S. Bengaard, J.K. Norskov, J. Sehested, B.S. Clausen, L.P. Nielsen, A.M. Molenbroek, J.R. Rostrup-Nielsen, J. Catal. **209**, 365 (2002)
24. J.K. Dahl, J. Tamburini, A.W. Weimer, Energ. Fuel **15**, 1227 (2001)
25. E.D. German, M. Sheintuch, J. Phys. Chem. C **117**, 22811 (2013)
26. D.C. Seets, C.T. Reeves, B.A. Ferguson, M.C. Wheeler, C.B. Mullins, J. Chem. Phys. **107**, 10229 (1997)
27. D.C. Seets, M.C. Wheeler, C.B. Mullins, J. Chem. Phys. **107**, 3986 (1997)
28. M.C.J. Bradford, M.A. Vannice, Catal. Rev. Sci. Eng. **41**, 1 (1999)
29. H.J. Freund, M.W. Roberts, Surf. Sci. Rep. **25**, 225 (1996)
30. S.G. Wang, X.Y. Liao, J. Hu, D.B. Cao, Y.W. Li, J. Wand, H. Jiao, Surf. Sci. **601**, 1271 (2007)
31. R.E. Reitmeier, K. Atwood, H.A. Bennett, H.M. Bauch, Ind. Eng. Chem. **40**, 620 (1948)
32. F. Abild-Pedersen, O. Lytken, J. Engbaek, G. Nielsen, I. Chorkendorff, J.K. Norskov, Surf. Sci. **590**, 127 (2005)
33. A.T. Bell, Science **299**, 1688 (2003)
34. G. Valderrama, C. Urbina de Navarro, M.R. Goldwasser, J. Power Sources **234**, 31 (2013)
35. J.R. Rostrup-Nielsen, Catal. Today **71**, 243 (2002)
36. B.C. Enger, R. Lodeng, A. Holmen, Appl. Catal. A **346**, 1 (2008)
37. R. Horn, K.A. Williams, N.J. Degenstein, A. Bitsch-Larsen, D. Dalle-Nogare, S.A. Tupy, L.D. Schmidt, J. Catal. **249**, 380 (2007)
38. D. Dalle-Nogare, N.J. Degenstein, R. Horn, P. Canu, L.D. Schmidt, J. Catal. **258**, 131 (2008)
39. J.D. Grunwaldt, S. Hannemann, C.G. Schroer, A. Baiker, J. Phys. Chem. B. **110**, 8674 (2006)
40. M. Maestri, D.G. Vlachos, A. Beretta, G. Groppi, E. Tronconi, J. Catal. **259**, 211 (2008)
41. A. Beretta, A. Donazzi, G. Groppi, M. Maestri, E. Tronconi, P. Forzatti, Catalysis **25**, 1 (2013)
42. R. Quiceno, J. Perez-Ramirez, J. Warnatz, O. Deutschmann, Appl. Catal. A **303**, 166 (2006)
43. A.B. Mhadeshwar, D.G. Vlachos, Ind. Eng. Chem. Res. **16**, 5310 (2007)
44. D. Dalle-Nogare, N.J. Degenstein, R. Horn, P. Canu, L.D. Schmidt, J. Catal. **277**, 134 (2011)

45. O. Korup, C.F. Goldsmith, G. Weinberg, M. Geske, T. Kandemir, R. Schlögl, R. Horn, J. Catal. **297**, 1 (2013)
46. H.J.M. Bouwmeester, Catal. Today **82**, 141 (2003)
47. G. Veser, Catal. Today **157**, 24 (2010)
48. X.X. Gao, C.J. Huang, N.W. Zhang, J.H. Li, W.Z. Weng, H.L. Wan, Catal. Today **131**, 211 (2008)
49. M. Aschi, M. Brönstrup, M.and Diefenbach, J.N. Harvey, D. Schröder, H. Schwarz, Angew. Chem. Int. Ed. **37**(6), 829 (1998)
50. R. Horn, G. Mestl, M. Thiede, F.C. Jentoft, P.M. Schmidt, M. Bewersdorf, R. Schlögl, Phys. Chem. Chem. Phys. **6**, 4514 (2004)
51. S. Delagrange, Y. Schuurman, Catal. Today **121**, 204 (2007)
52. S. Moehmel, N. Steinfeldt, S. Engelschalt, M. Holena, S. Kolf, M. Baerns, U. Dingerdissen, D. Wolf, R. Weber, M. Bewersdorf, Appl. Catal. A Gen. **334**, 73 (2008)
53. V.A. Kondratenko, Appl. Catal. A Gen. **381**, 74 (2010)
54. A.S. Bodke, D.A. Olschki, L.D. Schmidt, Appl. Catal. A **201**, 13 (2000)
55. G.E. Keller, M.M. Bhasin, J. Catal. **73**, 9 (1982)
56. W. Hinsen, M. Baerns, Chem.-Z. **107**, 223 (1983)
57. U. Zavyalova, M. Holena, R. Schlögl, M. Baerns, ChemCatChem **3**, 1935 (2011)
58. A.M. Maitra, Appl. Catal. A Gen. **104**, 11 (1993)
59. A.H. Tullo, Chem. Eng. News **92**, 20 (2014)
60. J.A. Labinger, Catal. Lett. **1**, 371 (1988)
61. D.J. Driscoll, W. Martir, J.X. Wang, J.H. Lunsford, J. Am. Chem. Soc. **107**, 58 (1985)
62. K.D. Campbell, J.H. Lunsford, J. Phys. Chem. **92**, 5792 (1988)
63. Y. Feng, J. Niiranen, D. Gutman, J. Phys. Chem. **95**, 6558 (1991)
64. Y. Feng, J. Niiranen, D. Gutman, J. Phys. Chem. **95**, 6564 (1991)
65. J.H. Lunsford, Angew. Chem. Int. Ed. **34**, 970 (1995)
66. S. Arndt, G. Laugel, S. Levchenko, R. Horn, M. Baerns, M. Scheffler, R. Schlögl, R. Schomäcker, Catal. Rev. Sci. Eng. **53**, 424 (2011)
67. P. Myrach, N. Nilius, S.V. Levchenko, A. Gonchar, T. Risse, K.P. Dinse, L.A. Boatner, W. Frandsen, R. Horn, H.J. Freund, R. Schlögl, ChemCatChem **2**, 854 (2010)
68. H. Schwarz, Angew. Chem. Int. Ed. **50**, 10096 (2011)
69. K. Kwapien, J. Paier, J. Sauer, M. Geske, U. Zavyalova, R. Horn, P. Schwach, A. Trunschke, R. Schlögl, Angew. Chem. Int. Ed. **53**, 8774 (2014)
70. P.F. Nelson, C.A. Lukey, N.W. Cant, J. Phys. Chem. **92**, 6176 (1988)
71. Q. Zhu, S.L. Wegener, C. Xie, O. Uche, M. Neurock, T.J. Marks, Nat. Chem. **5**, 104 (2013)
72. A.S. Hakemian, A.C. Rosenzweig, Annu. Rev. Biochem. **76**, 223 (2007)
73. J.A. Labinger, J. Mol. Catal. A **220**, 27 (2004)
74. A.V. de Vekki, S.T. Marakaev, Russ. J. Appl. Chem. **82**, 521 (2009)
75. A. Pamarliana, F. Arena, J. Catal. **167**, 57 (1997)
76. T.R. Baldwin, R. Burch, G.D. Squire, S.C. Tsang, Appl. Catal. **74**, 137 (1991)
77. H. Berndt, A. Martin, A. Brueckner, E. Schreier, D. Mueller, H. Kosslick, G.U. Wolf, B. Luecke, J. Catal. **191**, 384 (2000)
78. G. Du, S. Lim, Y. Yang, C. Wang, L. Pfefferle, G.L. Haller, Appl. Catal. A Gen. **302**, 48 (2006)
79. V. Fornés, C. López, H.H. López, A. Martínez, Appl. Catal. A Gen. **249**, 345 (2003)
80. Y. Li, D. An, Q. Zhang, Y. Wang, J. Phys. Chem. C **112**, 13700 (2008)
81. Q. Zhang, Y. Li, D. An, Y. Wang, Appl. Catal. A Gen. **356**, 103 (2009)
82. L.P. Didenko, V.R. Linde, V.I. Savchenko, Catal. Today **42**, 367 (1998)
83. L. Yu, S. Yuan, Z. Wu, J. Wan, M. Gong, G. Pan, Y. Chen, Appl. Catal. A Gen. **171**, L171 (1998)
84. A. Parmaliana, F. Arena, F. Frusteri, A. Mezzapica, Stud. Surf. Sci. Catal. **119**, 551 (1998)
85. X.L. Ding, Y.X. Zhao, X.N. Wu, Z.C. Wang, J.B. Ma, S.G. He, Chem. Eur. J. **16**, 11463 (2010)
86. Z.C. Wang, N. Dietl, R. Kretschmer, J.B. Ma, T. Weiske, M. Schlangen, H. Schwarz, Angew. Chem. Int. Ed. **51**, 3703 (2012)
87. A.E. Shilov, G.B. Shul'pin, Chem. Rev. **97**, 2879 (1997)
88. R.A. Periana, , G. Bhalla, W.J. Tenn, K.J.H. Young, X.J. Liu, O. Mironov, C.J. Jones, V.R. Ziatdinov, J. Mol. Catal. A **220**, 7 (2004)
89. R.A. Periana, D.J. Taube, E.R. Evitt, D.G. Löffler, P.R. Wentrcek, G. Voss, T. Masuda, Science **259**, 340 (1993)
90. R.A. Periana, D.J. Taube, S. Gamble, H. Taube, T. Satoh, H. Fujii, Science **280**, 560 (1998)
91. R. Palkovits, M. Antoniette, P. Kuhn, A. Thomas, F. Schüth, Angew. Chem. Int. Ed. **48**, 6909 (2009)
92. P.J. Smeets, J.S. Woertink, B.F. Sels, Solomon, R.A. Schoonheydt, Inorg. Chem. **49**, 3573 (2010)
93. M.H. Groothaert, J.A. van Bokhoven, A.A. Battiston, B.M. Weckhuysen, R.A. Schoonheydt, J. Am. Chem. Soc. **125**, 7629 (2003)
94. M.H. Groothaert, P.J. Smeets, B.F. Sels, P.A. Jacobs, R.A. Schoonheydt, J. Am. Chem. Soc. **127**, 1394 (2005)
95. J.S. Woertink, P.J. Smeets, M.H. Groothaert, M.A. Vance, B.F. Sels, R.A. Schoonheydt, E.I. Solomon, Proc. Natl. Acad. Sci. **106**, 18908 (2009)
96. E.M.C. Alayon, M. Nachtegaal, A. Bodi, J.A. van Bokhoven, J. A.Bokhoven, ACS Catal. **4**, 16 (2014)
97. E. Peringer, M. Salzinger, M. Hutt, A.A. Lemonidou, J.A. Lercher, Top. Catal. **52**, 1220 (2009)
98. V. Degirmenci, A. Yilmaz, U. Deniz, Catal. Today **142**, 30 (2009)
99. K.X. Wang, H.F. Xu, W.S. Li, X.P. Zhou, J. Mol. Catal. A-Chem. **225**, 65 (2005)
100. Z. Liu, W. Li, X. Zhou, J. Nat. Gas Chem. **19**, 522 (2010)
101. R. Lin, Y. Ding, L. Gong, J. Li, W. Chen, L. Yan, Y. Lu, Appl. Catal. A Gen. **353**, 87 (2009)
102. R. Lin, Y. Ding, L. Gong, W. Dong, W. Chen, Y. Lu, Catal. Today **164**, 34 (2011)
103. R. Wang, R. Lin, Y. Ding, J. Liu, J. Wang, T. Zhang, Appl. Catal. A Gen. **453**, 235 (2013)
104. R. Wang, R. Lin, Y. Ding, J. Liu, Catal. Lett. **144**, 1384 (2014)
105. Z.R. Ismagilov, E.V. Matus, L.T. Tsikoza, Energy Environ. Sci. **1**, 526 (2008)
106. S. Ma, X. Guo, L. Zhao, S. Scott, X. Bao, J. Energ. Chem. **22**, 1 (2013)
107. J.J. Spivey, G. Hutchings, Chem. Soc. Rev. **43**, 792 (2014)
108. P.M. Bijani, M. Sohrabi, S. Sahebdelfar, Chem. Eng. Technol. **35**, 1825 (2012)
109. H. Liu, S. Yang, S. Wu, F. Shang, X. Yu, C. Xu, J. Guan, Q. Kan, Energy **36**, 1582 (2011)
110. X. Guo, G. Fang, G. Li, H. Ma, H. Fan, L. Yu, C. Ma, X. Wu, D. Deng, M. Wei, D. Tan, R. Si, S. Zhang, J. Li, L. Sun, Z. Tang, X. Pan, X. Bao, Science **344**, 616 (2014)
111. B.Q. Xu, Natl. Sci. Rev. pp. 1–2 (2014)